JOURNAL OF SPACECRAFT AND ROCKETS
Vol. 47, No. 4, July–August 2010

Momentum Exchange Tether as a Hypersonic Parachute During Reentry for Human Missions

Jeffrey A. Kornuta* and S. M. Guo†
Louisiana State University, Baton Rouge, Louisiana 70803

DOI: 10.2514/1.48126

The use of tethers in space shows promise in future astronautical applications, with the strong possibility of providing more sophisticated functionality to satellites and spacecraft. One particular application of significant promise includes using a momentum exchange tether to deorbit a reentry capsule while simultaneously orbit-raising a base station. A possible consequence of this technology includes using the attached tether as a hypersonic parachute during reentry, effectively exploiting a momentum exchange tether as a drag device to reduce heat loads on the capsule. To quantify these benefits, the authors have investigated how various tether parameters would affect the system's performance in terms of reduced convective (aerothermal) heat fluxes and reduced temperatures on the capsule's leading edge, including the effect on the capsule's ballistic coefficient. Modeling the system as a series of lumped masses and rigid rods (links) in conjunction with Lagrange's equations, software was developed that is capable of generating the equations of motion for any arbitrary number of links. The resulting heat loads on the capsule were calculated using a one-dimensional multilayer heat transfer model based on the system's reentry dynamics. For certain cases, the presence of a tether can reduce the convective heat flux by almost 60% and the surface temperature by just over 20% when compared with an equivalent untethered system, which would be equivalent to an 80% reduction in capsule mass or a 60% increase in capsule diameter. Moreover, the ballistic coefficient for a tethered capsule may be reduced to almost 60 $\mathrm{kg/m^2}$ as compared with an untethered system value of 701 $\mathrm{kg/m^2}$.

Nomenclature

$\mathbf{a}$	=	acceleration, $\mathrm{m/s^2}$
$\hat{\mathbf{b}}$	=	tether segment-centered reference frame
C_D	=	drag coefficient
$\hat{\mathbf{c}}$	=	rotating reference frame
D	=	simplification parameter
d	=	tether diameter, mm
$\hat{\mathbf{e}}$	=	inertial reference frame
F	=	aerodynamic drag force, N
H	=	characteristic length, m
$\mathcal{H}$	=	hypersonic altitude range, km
h	=	capsule layer thickness, mm
K	=	heating coefficient, $\mathrm{kg^{1/2}/m}$
Kn	=	Knudson number
L	=	Lagrangian
ℓ	=	tether segment length, km
$\boldsymbol{M}$	=	system mass matrix
m	=	mass, kg
N	=	number of point masses
p	=	number of nonconservative forces
Q	=	nonconservative forces
q	=	generalized coordinate
q''	=	heat flux, $\mathrm{W/m^2}$
R	=	radial position, km
R_N	=	nose radius, m
S	=	drag frontal area, $\mathrm{m^2}$
T	=	kinetic energy
t	=	time, s
u	=	temperature, K
V	=	potential energy
$\mathbf{v}$	=	translational velocity, m/s
x	=	position within capsule layers, mm
α	=	tether angle, deg
β	=	ballistic coefficient, $\mathrm{kg/m^2}$
δ	=	signed direction
ε	=	emissivity
η	=	thermal diffusivity, $\mathrm{m^2/s}$
θ	=	angular position, deg
κ	=	thermal conductivity, W/m-K
λ	=	mean free path, m
μ	=	Earth's gravitational parameter, $\mathrm{m^3/s^2}$
ξ	=	radial distance along tether link, m
ρ	=	atmospheric density, $\mathrm{kg/m^3}$
σ	=	Stefan–Boltzmann constant, $\mathrm{W/m^2\text{-}K^4}$
Φ	=	bridging function
Ω	=	atmospheric angular velocity, rad/s
ω	=	angular velocity, rad/s

Subscripts:

c	=	capsule
f	=	skin friction
t	=	tether
w	=	with respect to wind
∞	=	freestream
$\parallel$	=	parallel to tether link
$\perp$	=	perpendicular to tether link

Received 15 November 2009; revision received 24 March 2010; accepted for publication 6 April 2010.

*Graduate Student, Department of Mechanical Engineering. Student Member AIAA.

†Assistant Professor, Department of Mechanical Engineering. Member AIAA.

I. Introduction

THE overall objective of this paper is to quantify the benefits of using a momentum exchange tether as a hypersonic parachute during the deorbiting of a reentry capsule from a base station. Specifically, the authors investigate the possible reduction in aerothermal heat flux and temperatures on the capsule as a result of reentry with an attached tether, including how various tether parameters affect these results. In this way, the utilization of a tethered space system (TSS) during reentry for human missions could reduce the overall cost of long-term space operations though

curtailing the amount of required fuel to perform a standard deorbit maneuver from the perspective of both the capsule and base station [1,2]. Furthermore, by remaining attached to the capsule after it is released from the base station, a momentum exchange tether could provide additional drag during the preparachute phase, effectively allowing it to act as a hypersonic parachute. As such, the presence of a tether during reentry could reduce mission costs by extending the lifetime of the capsule's heat shield or by reducing the capsule weight through removing unnecessary heat shield material.

Figure 1 depicts four separate phases for tether deployment and release. During Phase 1, the capsule is pushed away from the front of the station (pointing downward) with some initial velocity. Once Earth's gravity gradient has pulled the capsule to the desired tether length, the deployment mechanism is halted for Phase 2, causing the capsule to swing toward the local vertical. During Phase 3, the tether is severed at the deployer end once the capsule has reached the local relative equilibrium (local vertical). After severing the tether, Phase 4 begins as the capsule/tether system proceeds into a reentry trajectory toward Earth while the base station is put into a higher orbit (boosted) due to momentum conservation. It is noted that the amount of orbit boosting decreases as the station-to-capsule mass ratio increases.

The authors have only discovered one paper on the topic of modeling a capsule/tether reentry system. The paper, which was written by Krischke et al. about the capsule/tether system used in the 1993 SEDS-1 mission [3], describes the scenario of a reentry payload with an attached tether for use as a hypersonic parachute. Though Krischke et al. claim that the SEDS-1 payload could see a heat flux reduction up to 1 order of magnitude with a 20-km long, heat-resistant tether, there are notable dissimilarities with the system studied here. Not only is the capsule mass in the former analysis several orders of magnitude less than that which would be used for a human mission, but it only takes one particular tether geometry into account. Given these differences, additional analysis will need to be performed in order to study a capsule/tether reentry system for human missions.

The authors have dynamically modeled the TSS studied in this paper using a simplified lumped-mass approach due to the inherent complexity in solving the system's governing partial differential equations. By reconstructing the system as a series of lumped masses and rigid rods, one may use a more straight-forward method of obtaining the equations of motion (such as Lagrange's equations) while still capturing a majority of the system's dynamic characteristics. The authors have employed this method to find the governing system of ordinary differential equations (ODEs) resulting from Lagrange's equations.

II. Dynamic Modeling

A. Lagrangian Formulation

The following section describes the derivation of a dynamic capsule/tether system model in the presence of an atmosphere during reentry using Lagrange's equations. Similar to the system presented by Puig-Suari et al. [4], the capsule is modeled as a point mass, and the tether is modeled as N point masses adjoined by massless, rigid links in a two-dimensional, equatorial configuration space. The reference frame is given as $\hat{\mathbf{c}}$ and the inertial frame as $\hat{\mathbf{e}}$, and the two are Earth-centered and related through the relation $\boldsymbol{\omega}_{c/e} = \dot{\theta}\hat{\mathbf{c}}_3$. To begin modeling, Lagrange's equations are presented:

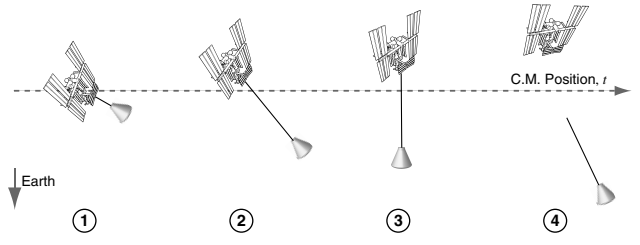

Fig. 1 Various phases of tether deployment and tether release.

$$\frac{\mathrm{d}}{\mathrm{d}t}\left(\frac{\partial L}{\partial \dot{q}_i}\right) - \frac{\partial L}{\partial q_i} = Q_i \tag{1}$$

where $L \equiv T - V$ and each Q_i represents the forces not derivable from a potential such as aerodynamic drag and other nonconservative forces. Each q_i represents a variable that describes the corresponding degree of freedom of the system. For this system, there are $N + 2$ degrees of freedom, which leads the configuration space, $\mathbf{q} \in \mathbb{R}^{(N+2)\times 1}$, to be described as

$$\mathbf{q} = [R \quad \theta \quad \alpha_1 \quad \alpha_2 \quad \ldots \quad \alpha_N]^T$$

To find L, both the kinetic energy, T, and the potential energy, V, must be found. The advantage of using the Lagrangian formulation for finding the equations of motion lies in its simplicity of derivation. In general, since $T = T(q, \dot{q})$ and $V = V(q)$, no accelerations need to be calculated in order to obtain the governing dynamic equations: only positions and velocities need to be found ($L \not\propto \ddot{q}$). Moreover, the expressions for both T and V may be expressed with respect to the local reference frame.

B. Equation Derivation

The kinetic energy of the system consists of contributions from both the capsule and each of the tether's point masses (Fig. 2). The kinetic energy for the capsule is given as

$$T_c = \frac{1}{2}m_c(\mathbf{v}_c \cdot \mathbf{v}_c) = \frac{1}{2}m_c(\dot{R}^2 + R^2\dot{\theta}^2) \tag{2}$$

since the position of the capsule is simply $R\hat{\mathbf{c}}_1$. The position of each ith mass of the tether is

$$\mathbf{R}_i = \left(R + \sum_{n=1}^{i} \ell_n \cos\alpha_n\right)\hat{\mathbf{c}}_1 + \left(\sum_{n=1}^{i} \ell_n \sin\alpha_n\right)\hat{\mathbf{c}}_2 \tag{3}$$

Accordingly, the velocity of each tether mass may be found:

$$\mathbf{v}_i = \frac{\mathrm{d}\mathbf{R}_i}{\mathrm{d}t} + \boldsymbol{\omega}_{c/e} \times \mathbf{R}_i = \left[\dot{R} - \sum_{n=1}^{i} \ell_n(\dot{\alpha}_n + \dot{\theta})\sin\alpha_n\right]\hat{\mathbf{c}}_1 + \left[R\dot{\theta} + \sum_{n=1}^{i} \ell_n(\dot{\alpha}_n + \dot{\theta})\cos\alpha_n\right]\hat{\mathbf{c}}_2 \tag{4}$$

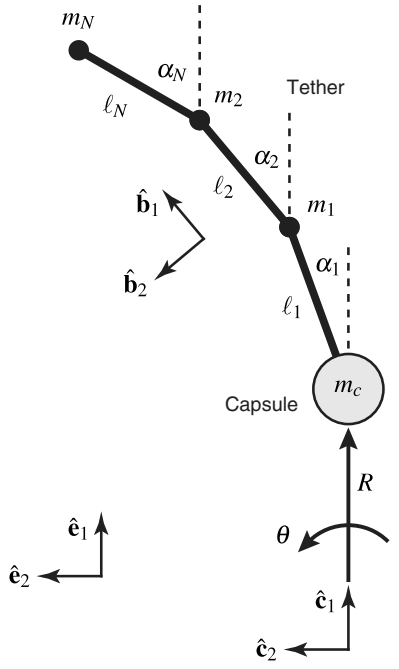

Fig. 2 Dynamic model of the TSS (adapted from Puig-Suari et al. [4]).

where ℓ_n is the same across all links (i.e. each segment has the same length). With the velocities in place, the kinetic energy of the tether is

$$T_t = \sum_{i=1}^{N}\left[\frac{1}{2}m_i(\mathbf{v}_i \cdot \mathbf{v}_i)\right] \tag{5}$$

Thus, the total kinetic energy is given as

$$\begin{aligned} T = T_c + T_t &= \frac{1}{2}m_c(\dot{R}^2 + R^2\dot{\theta}^2) \\ &+ \frac{1}{2}\sum_{i=1}^{N} m_i\left\{\left[\dot{R} - \sum_{n=1}^{i}\ell_n(\dot{\alpha}_n + \dot{\theta})\sin\alpha_n\right]^2\right. \\ &\left. + \left[R\dot{\theta} + \sum_{n=1}^{i}\ell_n(\dot{\alpha}_n + \dot{\theta})\cos\alpha_n\right]^2\right\} \end{aligned} \tag{6}$$

The system's potential energy stems from a Newtonian gravitational field:

$$V = -\mu\frac{m}{R} \tag{7}$$

where μ is the standard gravitational parameter and R is the distance from the center of Earth to the point in question. In this model, higher orders of the geopotential are ignored since the system is assumed to follow an equatorial path and the flight times are short. Thus, the potential energy of the capsule and each tether mass are

$$V_c = -\mu\frac{m_c}{R}, \qquad V_i = -\mu\frac{m_i}{\|\mathbf{R}_i\|}$$

respectively, where $\|\mathbf{R}_i\|$ is the radial distance from the reference frame, $\hat{\mathbf{c}}$, to the ith mass. From Eq. (3)

$$\begin{aligned} \|\mathbf{R}_i\| &= \sqrt{\mathbf{R}_i \cdot \mathbf{R}_i} \\ &= \left[\left(R + \sum_{n=1}^{i}\ell_n\cos\alpha_n\right)^2 + \left(\sum_{n=1}^{i}\ell_n\sin\alpha_n\right)^2\right]^{1/2} \end{aligned} \tag{8}$$

Thus, knowing $V = V_c + V_t$, we have

$$\begin{aligned} V &= -\mu\frac{m_c}{R} + \sum_{i=1}^{N} V_i \\ &= -\mu\frac{m_c}{R} - \mu\sum_{i=1}^{N} m_i\left[\left(R + \sum_{n=1}^{i}\ell_n\cos\alpha_n\right)^2\right. \\ &\left. + \left(\sum_{n=1}^{i}\ell_n\sin\alpha_n\right)^2\right]^{-1/2} \end{aligned} \tag{9}$$

In Lagrange's equations, each Q_i term represents the nonconservative forces exerted on the system. For instance, in this model, the Q_i terms only embody the aerodynamic drag exerted on both the capsule and the tether. Explained mathematically

$$Q_i = \sum_{k=1}^{p}\left(\mathbf{F}_k \cdot \frac{\partial \mathbf{R}_k}{\partial q_i}\right); \qquad i = \{1, 2, \ldots, N+2\} \tag{10}$$

where p is the number of nonconservative forces and $\mathbf{R}_k$ is the corresponding point of application for the kth force. It is noted that both $\mathbf{F}_k$ and $\mathbf{R}_k$ must be expressed in inertial coordinates.

In general, aerodynamic drag is described as

$$\mathbf{F}_D = -\frac{1}{2}\rho C_D S v_w \mathbf{v}_w \tag{11}$$

where C_D is the drag coefficient, S is the frontal area of the body, v_w is the velocity with respect to the atmosphere (wind) equal to $\|\mathbf{v}_w\|$, and ρ is the atmospheric density.

Assuming the atmosphere rotates with the planet at rate Ω, the velocity of the atmosphere with respect to the capsule, assuming an equatorial orbit, is

$$\mathbf{v}_{wc} = \dot{R}\hat{\mathbf{c}}_1 + R(\dot{\theta} - \Omega)\hat{\mathbf{c}}_2 \tag{12}$$

since $\boldsymbol{\omega}_{c/e} = (\dot{\theta} - \Omega)\hat{\mathbf{c}}_3$. Thus, the aerodynamic force on the capsule is

$$\begin{aligned} \mathbf{F}_c &= -\frac{1}{2}\rho_c C_{Dc} S_c\sqrt{\mathbf{v}_{wc} \cdot \mathbf{v}_{wc}}[\dot{R}\hat{\mathbf{c}}_1 + R(\dot{\theta} - \Omega)\hat{\mathbf{c}}_2] \\ &= F_{c1}\hat{\mathbf{c}}_1 + F_{c2}\hat{\mathbf{c}}_2 \end{aligned} \tag{13}$$

assuming no aerodynamic lift. Accordingly, since the capsule is assumed to be a point mass with a spherical body, the position describing the point of application for the capsule's drag force is as follows (in inertial coordinates):

$$\mathbf{R}_c = R\hat{\mathbf{c}}_1 = R(\cos\theta\hat{\mathbf{e}}_1 + \sin\theta\hat{\mathbf{e}}_2) \tag{14}$$

Using the above information, the generalized forces on the capsule can be identified using Eq. (10):

$$Q_{R,c} = \mathbf{F}_c \cdot \frac{\partial \mathbf{R}_c}{\partial R} = F_{c1} \tag{15}$$

$$Q_{\theta,c} = \mathbf{F}_c \cdot \frac{\partial \mathbf{R}_c}{\partial \theta} = RF_{c2} \tag{16}$$

while $Q_{\alpha_j,c} = 0$ since $\mathbf{R}_c \not\propto \alpha_j$.

The generalized forces on the tether must now be calculated. The differential force on the ith link at a distance, ξ, along the link (separated into normal and tangential components) is

$$\mathrm{d}\mathbf{F}_i = -\frac{1}{2}\rho_{\xi i} v_{w\xi i}\mathbf{v}_{w\xi i}(C_{D\xi i}\mathrm{d}S_\perp + C_{Df\xi i}\mathrm{d}S_\parallel) \tag{17}$$

where $\mathbf{v}_{w\xi i}$ is the velocity at the point, ξ, along the ith link with respect to the atmosphere. Both $C_{D\xi i}$ and $C_{Df\xi i}$ represent the pressure drag coefficient and skin friction drag coefficient, respectively. This velocity is described as

$$\begin{aligned} \mathbf{v}_{w\xi i} &= \left[\dot{R} - \xi(\dot{\alpha}_i + \dot{\theta} - \Omega)\sin\alpha_i\right. \\ &\left. - \sum_{n=1}^{i-1}\ell_n(\dot{\alpha}_n + \dot{\theta} - \Omega)\sin\alpha_n\right]\hat{\mathbf{c}}_1 \\ &+ \left[R(\dot{\theta} - \Omega) + \xi(\dot{\alpha}_i + \dot{\theta} - \Omega)\cos\alpha_i\right. \\ &\left. + \sum_{n=1}^{i-1}\ell_n(\dot{\alpha}_n + \dot{\theta} - \Omega)\cos\alpha_n\right]\hat{\mathbf{c}}_2 \end{aligned} \tag{18}$$

Both $\mathrm{d}S_\perp$ and $\mathrm{d}S_\parallel$ correspond to the differential areas perpendicular and parallel to the tether link, respectively:

$$\mathrm{d}S_\perp = d_i\mathrm{sgn}(\mathbf{v}_{w\xi i} \cdot \hat{\mathbf{b}}_2)\frac{\mathbf{v}_{w\xi i} \cdot \hat{\mathbf{b}}_2}{v_{w\xi i}}\,\mathrm{d}\xi \tag{19}$$

$$\mathrm{d}S_\parallel = \pi d_i\mathrm{sgn}(\mathbf{v}_{w\xi i} \cdot \hat{\mathbf{b}}_1)\frac{\mathbf{v}_{w\xi i} \cdot \hat{\mathbf{b}}_1}{v_{w\xi i}}\,\mathrm{d}\xi \tag{20}$$

where d_i is the diameter of the ith rod, and $\hat{\mathbf{b}}_1$ and $\hat{\mathbf{b}}_2$ are unit vectors along and normal to the tether segment, respectively. Using Eqs. (19) and (20) and substituting them back into the equation for $\mathrm{d}\mathbf{F}_i$ [Eq. (17)]

$$\begin{aligned} \mathrm{d}\mathbf{F}_i &= -\frac{1}{2}\rho_{\xi i} d_i[C_{D\xi i}\mathrm{sgn}(\mathbf{v}_{w\xi i} \cdot \hat{\mathbf{b}}_2)\mathbf{v}_{w\xi i} \cdot \hat{\mathbf{b}}_2 \\ &+ \pi C_{Df\xi i}\mathrm{sgn}(\mathbf{v}_{w\xi i} \cdot \hat{\mathbf{b}}_1)\mathbf{v}_{w\xi i} \cdot \hat{\mathbf{b}}_1]\mathbf{v}_{w\xi i}\,\mathrm{d}\xi \end{aligned} \tag{21}$$

For simplification purposes, the dot products in Eq. (21) are rewritten in terms of ξ:

$$\mathbf{v}_{w\xi i} \cdot \hat{\mathbf{b}}_2 = \mathbf{v}_{w\xi i} \cdot (\cos\alpha_i \hat{\mathbf{c}}_2 - \sin\alpha_i \hat{\mathbf{c}}_1) = D_1 + D_2\xi \tag{22}$$

$$\mathbf{v}_{w\xi i} \cdot \hat{\mathbf{b}}_1 = \mathbf{v}_{w\xi i} \cdot (\cos\alpha_i \hat{\mathbf{c}}_1 + \sin\alpha_i \hat{\mathbf{c}}_2) = D_3 + D_4\xi \tag{23}$$

where D_2 and D_4 represent terms proportional to ξ, and D_1 and D_3 represent terms not proportional to ξ. Additionally, we can assume that the expressions $\text{sgn}(\mathbf{v}_{w\xi i} \cdot \hat{\mathbf{b}}_2)$ and $\text{sgn}(\mathbf{v}_{w\xi i} \cdot \hat{\mathbf{b}}_1)$ do not change along each link, further simplifying the expressions by setting $\xi = 0$:

$$\text{sgn}\,(\mathbf{v}_{w\xi i} \cdot \hat{\mathbf{b}}_1) = \text{sgn}(D_3) = \delta_1 \tag{24}$$

$$\text{sgn}\,(\mathbf{v}_{w\xi i} \cdot \hat{\mathbf{b}}_2) = \text{sgn}(D_1) = \delta_2 \tag{25}$$

Substituting Eqs. (22–25) into Eq. (21), we have

$$\mathrm{d}\,\mathbf{F}_i = -\frac{1}{2}\rho_{\xi i} d_i [\delta_2 C_{D\xi i}(D_1 + D_2\xi) + \pi\delta_1 C_{Df\xi i}(D_3 + D_4\xi)]\mathbf{v}_{w\xi i}\,\mathrm{d}\xi \tag{26}$$

Unfortunately, due to the fact that the expressions for $\rho_{\xi i}$, $C_{D\xi i}$, and $\mathbf{v}_{w\xi i}$ are quite complex and depend on ξ, integrating Eq. (26) does not result in an analytical expression (Appendix A). However, for a large number of links, it should be reasonable to assume that $\mathbf{F}_i$ is constant along each link. Taking $\mathbf{F}_i(\xi) = \mathbf{F}_i(\ell_i/2)$, we have

$$\mathrm{d}\mathbf{F}_i = \left\{ -\frac{1}{2}\rho_{\xi i} d_i [\delta_2 C_{D\xi i}(D_1 + D_2\xi) + \pi\delta_1 C_{Df\xi i}(D_3 + D_4\xi)]\mathbf{v}_{w\xi i} \right\}_{\xi = \frac{\ell_i}{2}} \mathrm{d}\xi \tag{27}$$

Integrating Eq. (27) yields

$$\mathbf{F}_i = \int_0^{\ell_i} \mathrm{d}\mathbf{F}_i|_{\xi=\frac{\ell_i}{2}} = -\frac{1}{4}\rho_{i,1/2} d_i \ell_i \left[\delta_2 C_{Di,1/2}\left(D_1 + D_2\frac{\ell_i}{2}\right) + \pi\delta_1 C_{Dfi,1/2}\left(D_3 + D_4\frac{\ell_i}{2}\right)\right]\mathbf{v}_{wi,1/2} \tag{28}$$

where the subscript $(i, 1/2)$ represents the location $\xi = \ell/2$ of the ith link. At this point of application, the position vector is

$$\mathbf{R}_{i,1/2} = \left(R + \frac{\ell_i}{2}\cos\alpha_i + \sum_{n=1}^{i-1}\ell_i \cos\alpha_n\right)\hat{\mathbf{c}}_1 + \left(\frac{\ell_i}{2}\sin\alpha_i + \sum_{n=1}^{i-1}\ell_i \sin\alpha_n\right)\hat{\mathbf{c}}_2 \tag{29}$$

Of course, $\mathbf{F}_i$ and $\mathbf{R}_{i,1/2}$ must be written in inertial coordinates:

$$\mathbf{F}_i = \mathbf{F}_i \cdot (\cos\theta\hat{\mathbf{e}}_1 + \sin\theta\hat{\mathbf{e}}_2) \tag{30}$$

$$\mathbf{R}_{i,1/2} = \mathbf{R}_{i,1/2} \cdot (\cos\theta\hat{\mathbf{e}}_1 + \sin\theta\hat{\mathbf{e}}_2) \tag{31}$$

The generalized force expressions can now be found from the following:

$$Q_{R,t} = \sum_{j=1}^{N}\left(\mathbf{F}_j \cdot \frac{\partial \mathbf{R}_{j,1/2}}{\partial R}\right) \tag{32}$$

$$Q_{\theta,t} = \sum_{j=1}^{N}\left(\mathbf{F}_j \cdot \frac{\partial \mathbf{R}_{j,1/2}}{\partial \theta}\right) \tag{33}$$

$$Q_{\alpha_i,t} = \sum_{j=i}^{N}\left(\mathbf{F}_j \cdot \frac{\partial \mathbf{R}_{j,1/2}}{\partial \alpha_i}\right) \tag{34}$$

This leaves N terms in $Q_{\alpha_1,t}$, $N-1$ terms in $Q_{\alpha_2,t}$, two terms in $Q_{\alpha_{N-1},t}$, and one term in $Q_{\alpha_N,t}$. This completes the generalized force expressions, leaving the following for the system which has $N+2$ generalized coordinates and N tether links:

$$\begin{aligned}
Q_1 &= Q_{R,c} + Q_{R,t} = F_{c1} + \sum_{j=1}^{N}\left(\mathbf{F}_j \cdot \frac{\partial \mathbf{R}_{j,1/2}}{\partial R}\right)\\
Q_2 &= Q_{\theta,c} + Q_{\theta,t} = RF_{c2} + \sum_{j=1}^{N}\left(\mathbf{F}_j \cdot \frac{\partial \mathbf{R}_{j,1/2}}{\partial \theta}\right)\\
Q_3 &= Q_{\alpha_1,t} = \sum_{j=1}^{N}\left(\mathbf{F}_j \cdot \frac{\partial \mathbf{R}_{j,1/2}}{\partial \alpha_1}\right)\\
Q_4 &= Q_{\alpha_2,t} = \sum_{j=2}^{N}\left(\mathbf{F}_j \cdot \frac{\partial \mathbf{R}_{j,1/2}}{\partial \alpha_2}\right)\\
&\vdots\\
Q_{N+1} &= Q_{\alpha_{N-1},t} = \mathbf{F}_{N-1} \cdot \frac{\partial \mathbf{R}_{N-1,1/2}}{\partial \alpha_{N-1}} + \mathbf{F}_N \cdot \frac{\partial \mathbf{R}_{N-1,1/2}}{\partial \alpha_{N-1}}\\
Q_{N+2} &= Q_{\alpha_N,t} = \mathbf{F}_N \cdot \frac{\partial \mathbf{R}_{N,1/2}}{\partial \alpha_N}
\end{aligned} \tag{35}$$

C. Numerical Implementation

Once Lagrange's equations are found, we are left with $N+2$ second-order ODEs. To solve for these equations numerically, we need to convert the equations of motion into the form

$$\boldsymbol{M}\,\ddot{\mathbf{q}} = \mathbf{f}(\mathbf{q}, \dot{\mathbf{q}}, t) \tag{36}$$

where $\boldsymbol{M}$ is the system's mass matrix. Since the second-order derivatives of the generalized coordinates only arise from the $(\mathrm{d}/\mathrm{d}t)(\partial T/\partial \dot{q}_j)$ terms of Lagrange's equations [4], the elements of $\boldsymbol{M}$ may be found systematically by letting

$$\frac{\mathrm{d}}{\mathrm{d}t}\left(\frac{\partial T}{\partial \dot{q}_j}\right) \equiv \tilde{T}_{2j} + \tilde{T}_{1j} \tag{37}$$

where

$$\tilde{T}_{2j} \equiv \sum_{i=1}^{N+2} M_{ji}(\mathbf{q}, t)\ddot{q}_i, \qquad \tilde{T}_{1j} \equiv \frac{\mathrm{d}}{\mathrm{d}t}\left(\frac{\partial T}{\partial \dot{q}_j}\right) - \tilde{T}_{2j} \tag{38}$$

The $\ddot{q}_i$ terms may be systematically grouped into $\tilde{T}_{2j}$ either manually or through the use of computer algebra software such as Mathematica®. All other terms are placed within $\tilde{T}_{1j}$. In this way, the M_{ji} elements that comprise the mass matrix $\boldsymbol{M}$ may be found, and Eq. (36) may be solved using standard numerical packages after a first-order reduction is performed.

D. Initial Condition Generation via Dynamic Swing Release

To find the reentry system's initial conditions, the dynamics of the tether swing will be solved in order to find the conditions at tether release. As mentioned previously, the model of the capsule/tether system before reentry includes the time frame immediately after deployment ($\dot{\ell} = 0$, $\alpha \approx 45$ deg) to the moment right before tether termination ($\alpha = 0$). In this model (Fig. 3), the tether is assumed to be massless and rigid (henceforth referred to as inextensible) with the system again defined in an equatorial configuration space. Accordingly, running the simulation to find the system parameters at the release condition should give good approximate values for use as reentry phase initial conditions.

Since the release condition is defined by the point at which the capsule and tether are at the local vertical with respect to Earth ($\alpha = 0$), the authors have written a custom program in Mathematica that calculates the required parameters at this release position over various tether lengths by solving Lagrange's equations for the system model in Fig. 3 (assuming an initial altitude of 200 km for the system's center of mass and an equatorial orbit) [5]. The final result

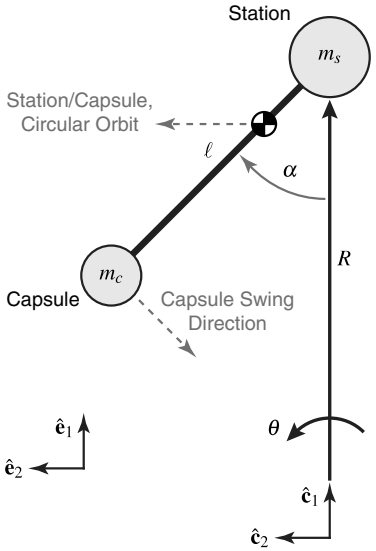

Fig. 3 Capsule/station system (dumbbell) model immediately before swing.

provided by this program is a function that returns the desired parameters (capsule position and velocity) when the user inputs a particular tether length. In this way, for any given tether length, an initial condition vector may be generated for a capsule/tether reentry simulation.

E. Capsule Heating

As the capsule/tether system is entering the atmosphere at hypersonic speeds, a thick boundary layer forms on the capsule surface and results in a strong bow shock that precedes the leading edge. Because of the high temperatures associated with this shock layer, there is a substantial amount of heat transfer into the reentry vehicle. The stagnation-point will be our point of interest since the leading edge of the blunt-bodied capsule will experience the brunt of the heat load.

Unfortunately, finding the resulting capsule temperatures requires knowledge of the surrounding flow field, which is difficult to solve since the high-temperature freestream fluid is not in equilibrium, chemically reacting, and possibly ionized. Though the governing equations that describe a compressible, stagnation-point boundary layer may be solved by themselves using a numerical shooting technique [6], a much more complex model that accounts for chemical dissociation and other molecular-level physics would also need to be considered. Because of these complexities, a simpler model will be used in order to perform a basic assessment.

Sutton and Graves developed a relationship that is frequently used to find the stagnation-point aerodynamic heat flux on a reentering body [7]. They accomplished this by numerically solving the boundary layer equations in chemical equilibrium to find the resulting (cold wall) convective heating. In this model, the stagnation-point convective heat flux is described as

$$q''_{\text{aero}} = K\sqrt{\frac{\rho}{R_N}}v^3 \tag{39}$$

where ρ is the freestream density, v is the freestream velocity, R_N is the nose radius, and $K \approx 1.83 \times 10^{-4}$ kg$^{1/2}$/m for Earth's atmosphere. Not only is this convective heating model widely used for reentry problems [3,8,9], but this $R_N^{-1/2}$ dependence describes why reentry vehicles must have a blunt shape to reduce aerodynamic heating.

To solve for the transient temperature profile at the stagnation-point, we will adopt a method similar to that of Meese and Nørstrud [9], who developed a simplified one-dimensional heat transfer conduction model for the surface of a reusable reentry vehicle. This abridged five-layer model accounts for both convective and radiative

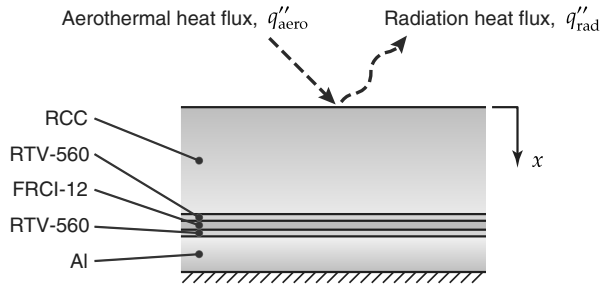

Fig. 4 One-dimensional heat transfer model for the capsule (detailed in Table 1).

effects at the surface while making the assumption that no heat escapes into the capsule interior (Table 1, Fig. 4). While it is noted that the incoming heat flux from Eq. (39) assumes a cold wall and the radiative heat loss assumes a hot wall, this heat transfer model should provide a reasonable estimation of the resulting temperature history.

Taking a control volume around the capsule layers, we have

$$\frac{\partial^2 u}{\partial x^2} = \frac{1}{\eta_x}\frac{\partial u}{\partial t} \tag{40}$$

where η_x is a piecewise function of the thermal diffusivity values in Table 1 based on location, x. The boundary conditions for Eq. (40) are

$$\frac{\partial u}{\partial x}(x=0,t) = -\frac{1}{\kappa_1}\left(K\sqrt{\frac{\rho}{R_N}}v^3 - \varepsilon\sigma u^4\right) \tag{41}$$

$$\frac{\partial u}{\partial x}(x=h_{\text{tot}},t) = 0 \tag{42}$$

where ε is the emissivity (assumed $\approx$0.85), σ is the Stefan–Boltzmann constant, κ_1 is the thermal conductivity of the first layer, and h_{tot} is the total thickness of all five capsule layers. The single initial condition is $u(x, t=0) = 294$ K, which is the temperature of the NASA space shuttle after several Earth orbits (with sunlight) before reentry [10]. It is noted that the temperatures of the tether will not be found in this model since the tether is assumed to remain intact throughout the entire simulation.

III. Results and Discussion

A. Literature Validation

Before proceeding with the analysis of a reentry capsule for human missions, the authors will first compare this method to the previously documented results for a reentering mass/tether system from Krischke et al. [3]. Figure 5 compares the numerical results of the authors' software to the results found in Krischke et al. for payload velocity versus altitude using the previously studied system parameters in Table 2.

Table 1 Capsule layer properties

Layer	Material	h, mm	κ, W/m-K	$\eta \times 10^6$, m^2/s
1	Reinforced carbon–carbon (RCC)	152.4	4.3	3.534
2	Room temperature vulcanizing adhesive (RTV-560)	2.0	0.424	0.2712
3	Fibrous refractory composite insulation (FRCI-12)	4.0	0.0505	0.2283
4	Room temperature vulcanizing adhesive (RTV-560)	2.0	0.424	0.2712
5	Aluminum (Al)	25.4	167.4	70.6

While the results between the authors' software and that of Krischke et al. agree qualitatively, we notice that there is some discrepancy between the two. These discrepancies are due to the fact that the authors' method only accounts for an endmass/tether system traveling in a two-dimensional equatorial trajectory, while the software of Krischke et al., a modified code originally developed at the Harvard–Smithsonian Center for Astrophysics called Master20 [11], takes into account a full three-dimensional trajectory. Accordingly, not only are the drag models different, but the previous model also includes perturbations such as the J_2 zonal harmonic of Earth's gravitational field to account for Earth's oblateness. Thus, it is difficult to make a direct comparison between the results of each piece of software.

Another disparity found in Fig. 5 lies with the wobbly nature of the authors' solution for a system which includes a tether. After some investigation, the authors have found that this irregularity is due to the fact that the payload's mass in this validation scenario is on the same order as the tether itself. In other words, the trajectory becomes more wobbly as the capsule mass approaches the tether mass (this phenomenon disappears as the capsule-to-tether mass ratio approaches and exceeds 10). Because of this size comparability, it is suspected that modeling more tether lumped masses would prevent this issue by providing better computational resolution (the authors' current reentry model uses four links). Fortunately, the mass of the capsule investigated in this paper is about two orders of magnitude heavier than the tether (Table 2), thus negating this issue.

B. Capsule/Tether Reentry System Analysis

The first system parameter to be analyzed is tether length. Figures 6 and 7 compare the effects of tether length on aerothermal heat flux and temperatures on the capsule surface for a corresponding inextensible tether swing release of that length (plots starting at a time value associated with an altitude of approximately 130 km). As expected, from Fig. 6 we see that increasing tether length does indeed reduce the convective heat flux on the capsule. However, for this tether diameter (1-mm) it is noted that there is a particular point at which the peak heat flux increases due to the fact that the slower release condition from a longer tether will cause a steeper reentry trajectory. This trend can be more easily seen in Fig. 8.

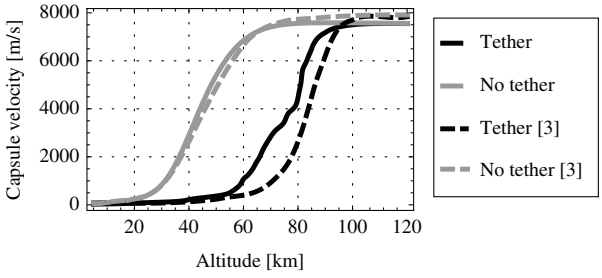

Fig. 5 Capsule velocity vs altitude validation (Krischke et al.).

Table 2 TSS parameters, including those used by Krischke et al. [3]

Parameter	Current	Krischke et al. [3]
Capsule mass	4,800 kg	23 kg
Capsule diameter	2.2 m	0.4 m
Initial orbit altitude	200 km	700 km
Station mass	15,000 kg	——
Release altitude	184.8–162.1 km	680 km
Release velocity	7749–7689 m/s	7,276 m/s
Tether material	Zylon[a]	Spectra
Tether density	1.56 g/cm^3	0.97 g/cm^3
Tether diameter	1 mm	1 mm
Tether links	4	7

[a]In practice, a 1-mm braided Zylon tether may not have a sufficient factor of safety for a human mission with capsule deorbiting using the presented capsule mass.

A more direct comparison between the tethered and untethered systems for an inextensible swing release can be made by considering differences in maximum heat flux and surface temperature due to the presence of a tether. Figure 8a reveals the percent decrease in the maximum convective heat flux experienced by the capsule due to the tether, while Fig. 8b reflects the percent decrease in maximum surface temperature of the capsule due to the tether. Though increasing tether length does indeed reduce aerodynamic heat flux, this reduction does not occur for each increasing tether length value. At these particular points, as mentioned previously, the slower release velocity caused by the increased tether length will force the system to enter the atmosphere slightly steeper. This steeper trajectory will, in turn, result in higher heat fluxes on the capsule. However, from observing the 1.5 and 2-mm diam tether results in Fig. 8, it is apparent that this temporary decrease in heat flux and surface temperature are soon overcome by the increased tether drag, and the overall trend indicates that increasing tether length does result in reduced heat loads.

The tether diameter also affects the heating of the capsule. The 1, 1.5, and 2-mm diameters are compared: Fig. 8a reveals the percent decrease in the maximum convective heat flux experienced by the capsule due to the tether, while Fig. 8b reflects the percent decrease in maximum surface temperature of the capsule due to the tether. Intuitively, the 2-mm tether performs best at reducing heat loads, offering almost 60% less convective heat flux and 20% less surface temperature in certain cases than an equivalent case without a tether.

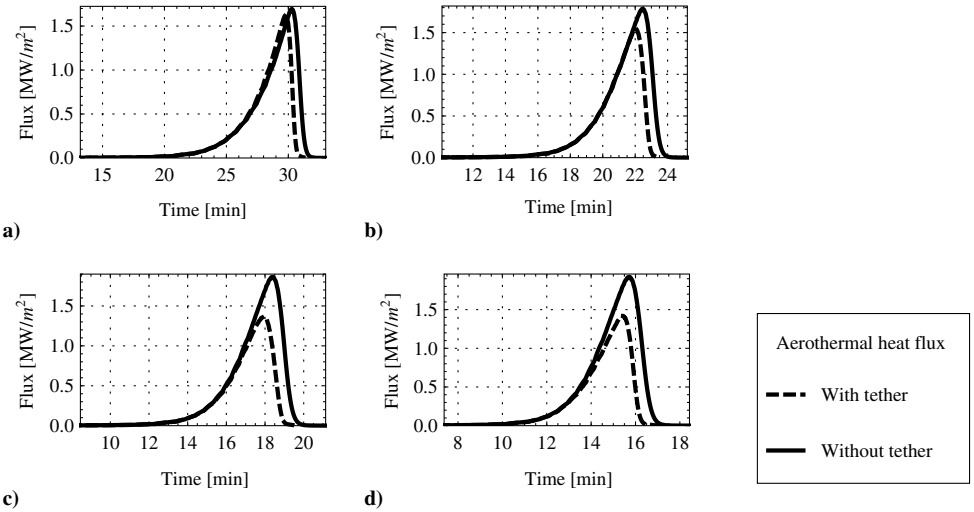

Fig. 6 Convective heat flux vs time and tether length for a 1-mm diam tether: a) $\ell = 20$ km, b) $\ell = 30$ km, c) $\ell = 40$ km, and d) $\ell = 50$ km.

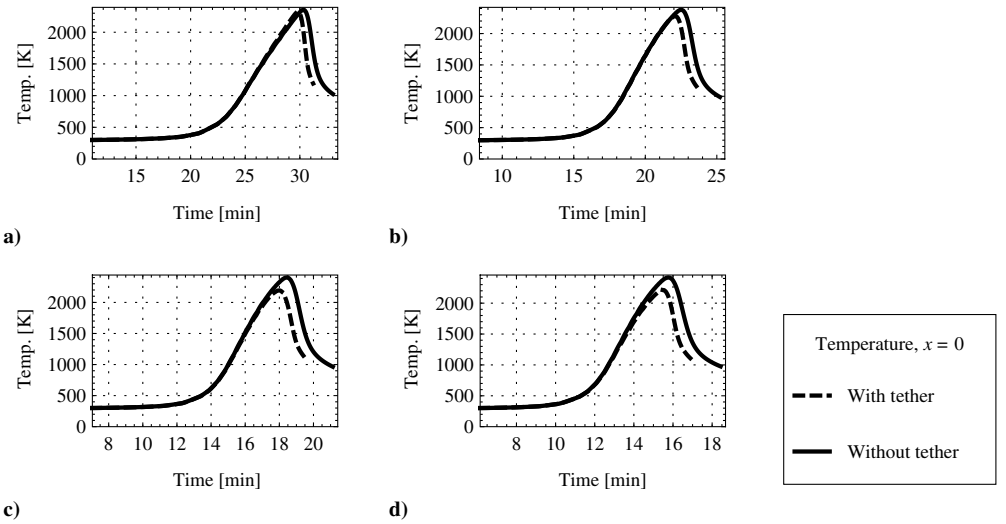

Fig. 7 Surface temperature ($x = 0$) vs time and tether length for a 1-mm diam tether: a) $\ell = 20$ km, b) $\ell = 0$ km, c) $\ell = 40$ km, and d) $\ell = 50$ km.

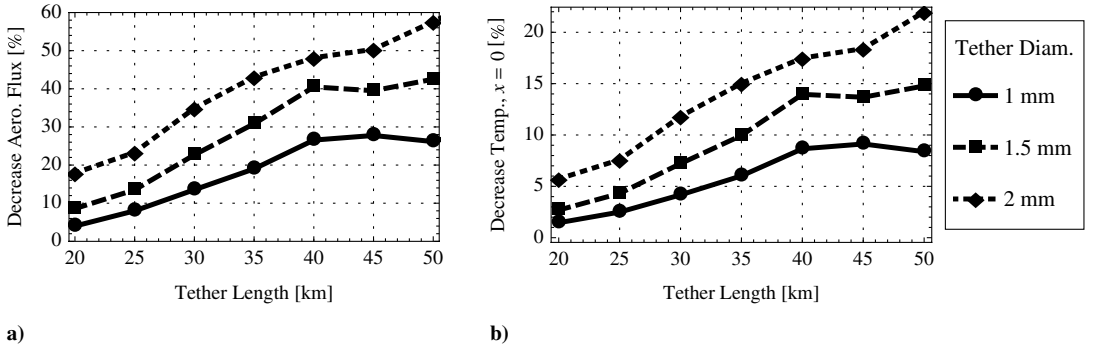

Fig. 8 Reduction in heat loads due to tether drag comparing tether length and diameter: a) percent decrease in maximum heat flux and b) percent decrease in maximum surface temperature.

To better understand the heat load reductions on the capsule, it is useful to observe the results in terms of an equivalent alteration in mass and diameter of an untethered capsule, holding all other parameters (including initial conditions for each tether length) constant. Figure 9a shows the equivalent percent decrease in capsule mass for untethered reentry given the surface temperature reductions shown in Fig. 8b. Alternatively, Fig. 9b displays the equivalent percent increase in capsule diameter for untethered reentry given the before-mentioned surface temperature reductions. For a 2-mm tether, the best-case reduction in maximum surface temperature is equivalent to an 80% reduction in untethered capsule mass and just over a 60% increase in untethered capsule diameter.

Additionally, the ballistic coefficient, defined as $\beta = m_c/C_D S$, is a valuable parameter that may be used to interpret the performance of the tether as a hypersonic parachute by describing the system's ability to overcome drag during reentry. Assuming a constant $C_{Dc} \approx 1.8$, the ballistic coefficient, β, of the reentry capsule without a tether is equal to 701 kg/m^2. Figure 10 shows an equivalent ballistic coefficient for the capsule/tether reentry system comparing both tether length and diameter [Eq. (B7), Appendix B]. As expected, the overall trends of Fig. 10 suggest that the ballistic coefficient will be reduced as both tether length and diameter are increased. The benefits of a tether are obvious: for a 2-mm diam tether, the equivalent ballistic coefficient of the capsule may be reduced to almost 60 kg/m^2.

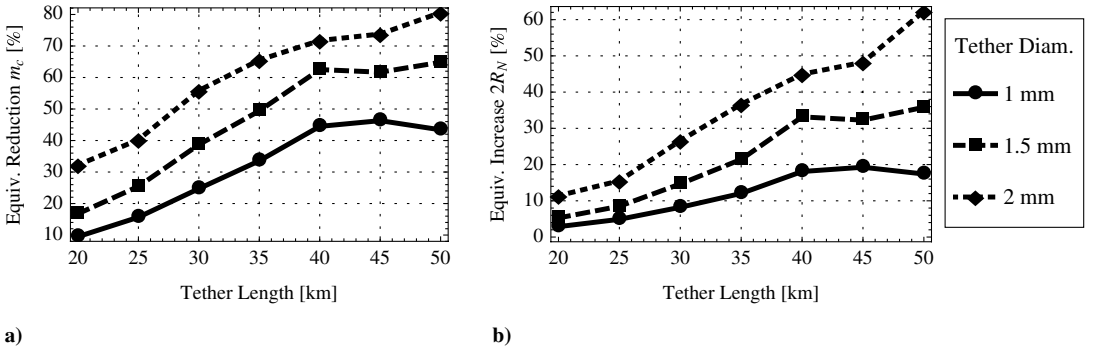

Fig. 9 Equivalent for an untethered capsule based on the surface temperature reductions found in Fig. 8b: a) percent decrease in capsule mass and b) percent increase in capsule diameter.

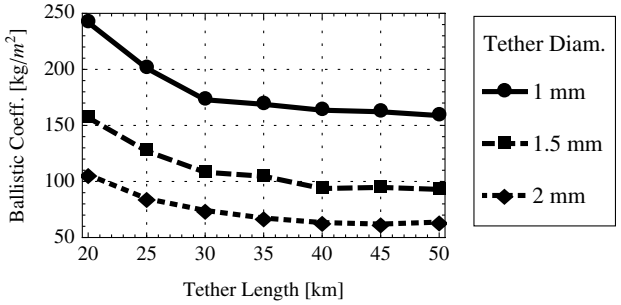

Fig. 10 Equivalent ballistic coefficient, β, for the capsule/tether reentry system comparing tether length and diameter (Appendix B).

IV. Conclusions

After using a momentum exchange tether to deorbit a reentry capsule, it is possible for the attached tether to benefit the system by serving as a hypersonic parachute during reentry. In this way, the role of a momentum exchange tether may effectively double as a drag device during reentry to reduce heat loads on the capsule. In this paper, the authors have investigated the possible reduction in convective (aerothermal) heat flux and temperatures on a capsule as a result of reentry with an attached momentum exchange tether, including how varying tether parameters affected these results.

After performing a thorough literature review, the authors determined that it was useful to develop software capable of simulating the reentering capsule/tether system. By modeling the system as a series of lumped masses and rigid rods (links) through the simplicity of Lagrange's equations, software was developed using Mathematica that was capable of generating the equations of motion for any arbitrary number of links. To solve the resulting equations of motion, a separate dynamic dumbbell station/capsule swing model was developed for a massless, inextensible tether to provide a realistic initial condition vector for the reentry phase. With the initial conditions in hand, the authors used the built-in numerical capabilities of Mathematica to solve the equations of motion numerically, allowing for a simple and effective software workflow.

For the analysis, the resulting motion of the capsule was solved in the case of varying tether length and tether diameter. Accordingly, using these reentry dynamics solutions for the system, the resulting heat loads on the capsule were calculated using a simplified one-dimensional multilayer heat transfer model. Thus, using this model, the incoming convective heat flux and temperature profile of the capsule material were found and analyzed for each of the dynamic cases.

As for the results, an increased tether length will ultimately reduce aerodynamic heat fluxes on the capsule. However, these reductions do not occur for each increasing tether length value: at these particular points, the slower release velocity will temporarily produce higher fluxes due to a steeper reentry trajectory. For a standard 1-mm tether diameter, the presence of a tether can decrease the convective heat flux on the capsule by almost 30% while decreasing the surface temperature by almost 10%. Additionally, increased tether diameter also decreases aerodynamic heat fluxes and surface temperatures. For the 2-mm diam case, the convective heat flux into the capsule can be reduced by almost 60% and the surface temperature by just over 20% when compared with an equivalent system without a tether. Consequently, the optimum reduction in maximum surface temperature is equivalent to an 80% reduction in capsule mass or just over a 60% increase in capsule diameter during untethered reentry. Furthermore, the ballistic coefficient, a useful parameter in assessing the ability of a reentry vehicle to overcome drag, is found to decrease with both increasing tether length and diameter. For a capsule with a 2-mm diam tether, the ballistic coefficient could be reduced to almost 60 kg/m^2 when compared with an untethered system value of 701 kg/m^2.

With these observed heat load reductions, it is apparent that a momentum exchange tether could reduce heat loads substantially on a capsule during reentry for human missions. As such, in addition to providing an efficient means of performing a deorbit maneuver, a heat-resistant tether may also serve as an effective hypersonic parachute for a human reentry mission by possibly increasing the lifetime of the capsule or by reducing the amount of required heat shield material. Additional factors to be considered for an effective hypersonic parachute, such as the fatigue properties of the capsule's heat shield, the predictability of the reentry trajectory, or an assessment of the system's overall safety, are not addressed in this study.

Appendix A: Drag Coefficient Data

Though $\rho_{\xi i}$ could reasonably be assumed to be an exponential function, the combination of $\rho_{\xi i}$, $C_{D\xi i}$, and $v_{w\xi i}$ would still prevent the expression, $d\mathbf{F}_i$, from being integrated in a straight-forward manner [Eq. (26)]. $C_{D\xi i}$ is particularly complex due to its dependence on ξ through the Knudson number, $Kn = \lambda_\infty / H$, where H is the characteristic length of the capsule (the diameter) and λ_∞ is the mean free path of the freestream flow.

Following Gallais [8], a pressure drag coefficient approximation, which is taken to be the same for both the capsule (a sphere) and the tether (a cylinder), for a reentry vehicle may be approximated by

$$C_D = C_{\text{con}} + \Phi(Kn_\infty)(C_{\text{mol}} - C_{\text{con}}) \tag{A1}$$

where C_{con} is the drag coefficient at continuum conditions ($\approx$1), C_{mol} is the drag coefficient at molecular conditions ($\approx$2), and Φ is a bridging function:

$$\Phi(Kn_\infty) = \frac{1}{2}\left[1 + \text{erf}\left(\frac{\sqrt{\pi}}{\Delta Kn}\,\ell_n\left(\frac{Kn_\infty}{Kn_{\text{mi}}}\right)\right)\right] \tag{A2}$$

In Eq. (A2), $\Delta Kn = \ell_n\, Kn_{\text{mol}} - \ell_n\, Kn_{\text{con}}$ is the logarithmic width of the intermediate zone, $Kn_{\text{mol}} \approx 10$, $Kn_{\text{con}} \approx 10^{-2}$, and Kn_{mi} is the middle value of the intermediate zone ($\approx$0.5 for a Soyuz-type geometry) [8]. The skin friction drag coefficient is taken to be a constant ($\approx 10^{-2}$) due to its smaller influence compared with the pressure drag coefficient.

Appendix B: Equivalent Ballistic Coefficient Derivation

It is difficult to calculate the ballistic coefficient for a reentering capsule/tether system due to the highly dynamic motion of the tether during the reentry trajectory. The ballistic coefficient is given in Eq. (B1):

$$\beta = \frac{m_c}{C_D S} \tag{B1}$$

Studying Eq. (B1), it is apparent that the denominator, $C_D S$, for a capsule/tether system is not a direct calculation. Unlike that of a standalone reentry capsule, a capsule/tether system will exhibit a highly-varying $C_D S$ term. Thus, the authors will proceed to find an equivalent $C_D S$ term for a reentry capsule with an attached tether in order to calculate β.

To account for the additional drag a tether provides to the reentry capsule, the tether force acting on the capsule must be found. The tether force may be calculated by performing a force balance on the capsule:

$$\mathbf{F}_t = m_c \mathbf{a}_c - \mathbf{F}_{D,c} + \mu m_c \frac{\mathbf{R}}{R^3} \tag{B2}$$

where $\mathbf{F}_t$ is the tether force, $\mathbf{a}_c$ is the acceleration of the capsule, $\mathbf{F}_{D,c}$ is the drag force on the capsule, and $-\mu m_c \mathbf{R}/R^3$ is Earth's gravitational force on the capsule. Additionally, we are only interested in the tether force acting in the capsule drag direction:

$$F_{D,t} = \mathbf{F}_t \cdot \frac{\mathbf{F}_{D,c}}{\|\mathbf{F}_{D,c}\|} \tag{B3}$$

Thus, the total force acting on the capsule in the drag direction is

$$F_{D,t} + F_{D,c} = \frac{1}{2}\rho_c(\mathbf{v}_{wc} \cdot \mathbf{v}_{wc}) C_{Dc} S_c \tag{B4}$$

which may then be rearranged to yield

$$C_{Dc}S_c = \frac{2(F_{D,t} + F_{D,c})}{\rho_c(\mathbf{v}_{wc} \cdot \mathbf{v}_{wc})} \tag{B5}$$

Because Eq. (B5) varies greatly with altitude during reentry, an equivalent $C_{Dc}S_c$ term will be calculated by integrating (numerically) over the hypersonic portion of the trajectory, $\mathcal{H}$ (altitudes $\gtrsim$25 km):

$$C_{Dc}S_c|_{\text{equiv}} = \frac{1}{\mathcal{H}} \int_{\mathcal{H}} \frac{2(F_{D,t} + F_{D,c})}{\rho_c(\mathbf{v}_{wc} \cdot \mathbf{v}_{wc})}\, \mathrm{d}R \tag{B6}$$

Thus, an equivalent ballistic coefficient for the capsule/tether system may be found:

$$\beta|_{\text{equiv}} = \frac{m_c}{C_{Dc}S_c|_{\text{equiv}}} \tag{B7}$$

Acknowledgments

The authors would like to thank Excalibur Almaz for funding this research. They also thank Leroy Chiao of Exalibur Almaz and Robert Hoyt of Tethers Unlimited for their mentoring, insight, and support on this project.

References

[1] Carroll, J. A., "Tether Applications in Space Transportation," *Acta Astronautica*, Vol. 13, No. 4, 1986, pp. 165–174. doi:10.1016/0094-5765(86)90061-5

[2] Johnson, L., Gilchrist, B., Estes, R. D., and Lorenzini, E., "Overview of Future NASA Tether Applications," *Advances in Space Research*, Vol. 24, No. 8, 1999, pp. 1055–1063. doi:10.1016/S0273-1177(99)00553-0

[3] Krischke, M., Lorenzini, E., and Sabath, D., "A Hypersonic Parachute for Low-Temperature Re-Entry," *Acta Astronautica*, Vol. 36, No. 5, 1995, pp. 271–278. doi:10.1016/0094-5765(95)00108-C

[4] Puig-Suari, J., Longuski, J. M., and Tragesser, S. G., "Aerocapture with a Flexible Tether," *Journal of Guidance, Control, and Dynamics*, Vol. 18, No. 6, 1995, pp. 1305–1312. doi:10.2514/3.21546

[5] Kornuta, J. A., Dynamical Investigation of a Manned Capsule/Tether Re-Entry System, Master's Thesis, Louisiana State Univ., Baton Rouge, LA, 2009.

[6] Anderson, J. D., Jr., *Fundamentals of Aerodynamics*, 4th ed., McGraw–Hill, New York, 2007, pp. 848–850.

[7] Sutton, K., and Graves, R. A., Jr., "A General Stagnation-Point Convective-Heating Equation for Arbitrary Gas Mixtures," NASA, TR R-376, 1971.

[8] Gallais, P., *Atmospheric Re-Entry Vehicle Mechanics*, Springer–Verlag, Berlin, 2007, pp. 56–57,151.

[9] Meese, E. A., and Nørstrud, H., "Simulation of Convective Heat Flux and Heat Penetration for a Spacecraft at Re-Entry," *Aerospace Science and Technology*, Vol. 6, No. 3, 2002, pp. 185–194. doi:10.1016/S1270-9638(02)01165-3

[10] Windhorst, R., Ardema, M., and Bowles, J., "Minimum Heating Entry Trajectories for Reusable Launch Vehicles," *Journal of Spacecraft and Rockets*, Vol. 35, No. 5, 1998, pp. 672–682. doi:10.2514/2.3384

[11] Lorenzini, E., "Quarterly Report No. 5, NASA Contract NAS8-36606," Smithsonian Inst. Astrophysical Observatory, Cambridge, MA, 1986.

C. Kluever
Associate Editor